Transp Porous Med (2013) 98:223–238
DOI 10.1007/s11242-013-0142-1

Natural Convection Induced by a Heated Vertical Plate Embedded in a Porous Medium with Transpiration: Local Thermal Non-equilibrium Similarity Solutions

Mohsen Nazari · Esmaeel Shakerinejad · Morteza Nazari · D. Andrew S. Rees

Received: 23 August 2012 / Accepted: 6 February 2013 / Published online: 22 February 2013

Abstract This paper is concerned with the thermal non-equilibrium free convection boundary layer, which is induced by a vertical heated plate embedded in a saturated porous medium. The effect of suction or injection on the free convection boundary layer is also studied. The plate is assumed to have a linear temperature distribution, which yields a boundary layer of constant thickness. On assuming Darcy flow, similarity solutions are obtained for governing the steady laminar boundary layer equations. The reduced Nusselt numbers for both the solid and fluid phases are calculated for a wide range of parameters, and compared with asymptotic analyses.

Keywords Thermal non-equilibrium · Natural convection · Porous medium · Similarity solution

List of symbols

A	Constant
C	Constant
f	Reduced streamfunction
f_w	Suction parameter
F	Reduced streamfunction in Appendix A
g	Gravity
h	Dimensional interstitial heat transfer coefficient
H	Nondimensional interstitial heat transfer coefficient

M. Nazari · E. Shakerinejad
Department of Mechanical Engineering, Shahrood University of Technology, Shahrood, Iran

M. Nazari
Department of Mathematics, Shahrood University of Technology, Shahrood, Iran

D. A. S. Rees (✉)
Department of Mechanical Engineering, University of Bath, Bath BA2 7AY, UK
e-mail: D.A.S.Rees@bath.ac.uk

k	Thermal conductivity
K	Permeability
LTE	Local thermal equilibrium
LTNE	Local thermal non-equilibrium
Nu	Local Nusselt number
q	Surface rate of heat flux
Ra_x	Local Darcy-Rayleigh number
T	Dimensional temperature
u	Vertical velocity
v	Horizontal velocity
x	Vertical coordinate
y	Horizontal coordinate

Greek Characters

α	Thermal diffusivity
β	Thermal expansion coefficient
γ	Porosity-modified conductivity ratio
δ	Constant
ϵ	Porosity
ζ	Scaled similarity variable
η	Similarity variable
θ	Nondimensional fluid temperature
Θ	Inner-layer fluid temperature
ν	Kinematic viscosity
ξ	Scaled similarity variable
ρ	Density
τ	Constant
ϕ	Nondimensional solid temperature
Φ	Inner-layer solid temperature
ψ	Streamfunction

Superscripts and Subscripts

∞	Ambient/initial conditions
$\cdot$	Derivative with respect to ζ
$'$	Derivative with respect to η
f	Fluid
p	Constant pressure
s	Solid
w	Wall

1 Introduction

The study of the natural convection flow and heat transfer from surfaces that are held at a temperature which is different from the ambient porous medium has been of considerable interest in energy-related engineering problems for many decades. The first papers to consider

the resulting boundary layer flows were by Cheng and Minkowycz (1977), who considered convection induced by a hot vertical surface, and Cheng and Chang (1976), who studied the corresponding horizontal boundary layer. Both configurations yield self-similar solutions.

The great majority of papers which study such problems usually adopt a single field equation for the temperature field of the porous medium. But very recent work has been concerned with relaxing the assumption that the local temperatures of the solid and fluid phases are equal. A simple example where this situation might arise is when a hot fluid is suddenly injected into a cold porous medium, and it takes time for the mean temperatures of the phases at any chosen point to tend towards the same value; see Rees et al. (2008) and Rees and Bassom (2010) for examples of such cases.

However, such a lack of local thermal equilibrium (LTE) is not confined to unsteady flows. Steady-state examples include cavity convection studied by both Baytaş and Pop (2002) and Mohamad (2000), Darcy-Bénard convection by Combarnous and Bories (1974) and Banu and Rees (2002), and the local thermal non-equilibrium (LTNE) analogue of the vertical boundary layer of Cheng and Minkowycz (1977) by Rees and Pop (2000) and Rees (2003). In all of these cited papers, LTNE is modelled by two separate equations of heat transport, one for the fluid phase and one for the solid phase. The interstitial transfer of heat between the phases is modelled macroscopically by a simple source/sink term which is proportional to the local temperature difference between the phases. Reviews of these matters may be found in Kuznetsov (1998) and Rees and Pop (2005).

In the present paper we consider the combined effects of LTNE, uniform surface suction/blowing and buoyancy due to the presence of linear variations of the temperature on the buoyancy-induced flow from a vertical surface. This yields a boundary layer of constant thickness, a thermal analogue of Heimenz flow at a stagnation point. The similarity solutions have to be solved numerically, and this forms the focus of the present paper, but when LTNE, surface suction/blowing and temperature variations are absent, the governing equations may be solved analytically. Our work extends the previous paper by Cheng (1977).

2 Governing Equations and Basic Solution

We consider a vertical flat plate embedded in a saturated porous medium, as shown in Fig.1. The plate may be permeable ($v_w \neq 0$) or impermeable ($v_w = 0$). A linearly varying temperature distribution is imposed on the surface of the plate according to $T_w = T_\infty + Ax$, where the ambient condition far from the wall is that $T = T_\infty$. The constant, A, is positive and this corresponds to the case where, for an impermeable heated surface, fluid is drawn towards the plate from large values of y and there is a stagnation point at $x = 0$.

The fluid properties are assumed to be constant except for density variations in the buoyancy force term, and we assume that the Boussinesq approximation applies. The governing equations allow for the presence of local thermal non-equilibrium effects and we assume that the flow is described well by the Darcy model. Thus, the full boundary layer equations for the flow of an incompressible viscous fluid are given as,

$$\frac{\partial u}{\partial x} + \frac{\partial v}{\partial y} = 0, \tag{1}$$

$$\frac{\partial u}{\partial y} = \frac{gK}{\nu}\beta\frac{\partial T_f}{\partial y}, \tag{2}$$

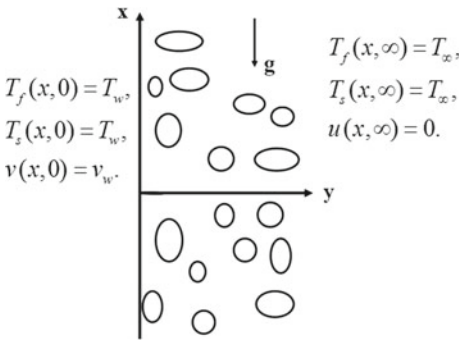

Fig. 1 Definition sketch of the configuration being studied

$$u\frac{\partial T_\mathrm{f}}{\partial x}+v\frac{\partial T_\mathrm{f}}{\partial y}=\epsilon\alpha_\mathrm{f}\frac{\partial^2 T_\mathrm{f}}{\partial y^2}+\frac{h}{(\rho c_\mathrm{p})_\mathrm{f}}(T_\mathrm{s}-T_\mathrm{f}), \tag{3}$$

$$(1-\epsilon)\alpha_\mathrm{s}\frac{\partial^2 T_\mathrm{s}}{\partial y^2}+\frac{h}{(\rho c_\mathrm{p})_\mathrm{s}}(T_\mathrm{f}-T_\mathrm{s})=0, \tag{4}$$

where the Cartesian coordinates, x and y, are measured along the plate and normal to it respectively, u and v are the velocity components in the x and y directions, respectively, T is the temperature, ϵ is porosity, ν, the kinematic viscosity of the fluid, and β the coefficient of thermal expansion. In Eqs. (3) and (4) the value, h, is the interstitial heat transfer coefficient between the solid and fluid phases. When h takes sufficiently large values, then T_f and T_s are almost equal and the phases are deemed to be in LTE. On the other hand, for other values of h, the temperatures of the phases are locally different and LTNE conditions are said to prevail. A comprehensive set of analytical and numerical values of h for different porous microstructures and conductivity ratios for stagnant media may be found in Rees (2009, 2010), while some correlations for non-stagnant cases have been quoted in Rees and Pop (2005).

The boundary conditions are,

$$y=0: \quad T_\mathrm{f}=T_\mathrm{s}=T_\mathrm{w}(x)=T_\infty+Ax, \quad v=v_\mathrm{w}, \tag{5}$$

$$y\to\infty: \quad T_\mathrm{f},T_\mathrm{s}\to T_\infty, \qquad\qquad u\to 0. \tag{6}$$

It proves convenient to introduce the following transformations,

$$\theta=\frac{T_\mathrm{f}-T_\infty}{T_\mathrm{w}-T_\infty}, \quad \phi=\frac{T_s-T_\infty}{T_\mathrm{w}-T_\infty}, \tag{7}$$

$$\psi=\epsilon\,\alpha_\mathrm{f}\,\mathrm{Ra}_x^{1/2}f(\eta), \quad u=\frac{\partial\psi}{\partial y}=\epsilon\left(\frac{\alpha_\mathrm{f}}{x}\right)\mathrm{Ra}_x f'(\eta), \quad v=-\frac{\partial\psi}{\partial x}=-\epsilon\left(\frac{\alpha_\mathrm{f}}{x}\right)\mathrm{Ra}_x^{1/2}f(\eta), \tag{8}$$

where

$$\mathrm{Ra}_x=\frac{g\beta K(T_\mathrm{w}-T_\infty)x}{\epsilon\nu\alpha_\mathrm{f}}\,\frac{g\beta KAx^2}{\epsilon\nu\alpha_\mathrm{f}} \tag{9}$$

is the local Darcy-Rayleigh number, and where

$$\eta=\mathrm{Ra}_x^{1/2}\frac{y}{x} \tag{10}$$

is the similarity variable. Given the definition of Ra_x this means that η is a scaled version of y and the boundary layer has constant thickness. On substituting Eqs. (7)–(10) into Eqs. (2)–(4), we obtain the following equations for the similarity solution,

$$f'' = \theta', \tag{11}$$

$$\theta'' + f\theta' - f'\theta = H(\theta - \phi), \tag{12}$$

$$\phi'' = H\gamma(\phi - \theta), \tag{13}$$

and the boundary conditions become,

$$\eta = 0: \quad f = f_\mathrm{w}, \quad \theta = \phi = 1, \tag{14}$$

$$\eta \to \infty: \quad f', \theta, \phi \to 0. \tag{15}$$

Equations (11)–(15) form a three-parameter system of equations where the parameters are f_w, H and γ. The value, f_w, is the suction parameter. A zero value of f_w corresponds to an impermeable surface, a positive value to a suction surface and a negative value to a blowing surface. The other two are

$$H = \frac{hx^2}{\epsilon k_\mathrm{f} \mathrm{Ra}_x} \quad \text{and} \quad \gamma = \frac{\epsilon k_\mathrm{f}}{(1-\epsilon)k_\mathrm{s}}; \tag{16}$$

these are the interstitial heat transfer parameter and the porosity-modified conductivity ratio, respectively. Both of these parameters are constants.

The heat fluxes at the surface may be written in the form,

$$q_\mathrm{f} = -k_\mathrm{f} \frac{\partial T_\mathrm{f}}{\partial y}\Big|_{y=0}, \quad q_\mathrm{s} = -k_\mathrm{s} \frac{\partial T_s}{\partial y}\Big|_{y=0}. \tag{17}$$

After scaling these expressions become,

$$q_\mathrm{f} = -\frac{k_\mathrm{f}(T_\mathrm{w} - T_\infty)\mathrm{Ra}_x^{1/2}}{x}\theta'(0), \quad q_\mathrm{s} = -\frac{k_\mathrm{s}(T_\mathrm{w} - T_\infty)\mathrm{Ra}_x^{1/2}}{x}\phi'(0). \tag{18}$$

Therefore we may define the following reduced Nusselt numbers,

$$\mathrm{Nu}_\mathrm{f}\mathrm{Ra}_x^{-1/2} = \frac{x}{k_\mathrm{f}(T_\mathrm{w} - T_\infty)} q_\mathrm{f} = -\theta'(0), \quad \mathrm{Nu}_\mathrm{s}\mathrm{Ra}_x^{-1/2} = \frac{x}{k_\mathrm{s}(T_\mathrm{w} - T_\infty)} q_\mathrm{s} = -\phi'(0) \tag{19}$$

3 Numerical Methods

The system of governing equations and their boundary conditions, Eqs. (11)–(15), were solved using two different numerical methods to provide cross-correlation for accuracy of coding. One of these was the classical fourth-order Runge-Kutta method allied with the shooting technique, while the other was a slightly modified version of Keller's box method, where one of the non-dimensional parameters played the role of the marching coordinate, thereby allowing solutions to be obtained easily for a range of values of that parameter.

Solutions using the Runge-Kutta method adopted 100 uniformly spaced grid points, whereas the Keller box method (a second order method) used up to 400 grid points on a non-uniform grid which was fine near $\eta = 0$ and which became less so as η increases with

a grid expansion factor of 1.04. Solutions obtained by the two methods were compared and found to agree very closely. Most of the computations presented here, especially those for small values of H (for which the thermal boundary layers of the two phases differ greatly in their thicknesses), were obtained using the Keller box method.

Solutions have been obtained for different values of f_w, H and γ. It was found that the width of the boundary layer depends on the magnitude of the parameters. Thus, small values of either H or γ cause the thermal boundary layer thickness of the solid phase to be much greater than that of the fluid phase. Strong suction at the surface causes the thermal boundary layer thickness of the fluid phase to be very thin compared with that of the solid phase. Blowing from the surface increases the boundary layer thicknesses compared with those for suction or when the surface is impermeable. Therefore the particular value of η_{max} which was used in our computations depended on the values of the parameters, and each was selected subject to the requirement that the boundary layers were well-contained within the computational domain and sufficiently well-resolved.

One test of the accuracy of the present numerical simulations is provided by setting $H = 0$ in Eqs. (11) and (12) and by ignoring the variation of ϕ. These are, in effect, the equations which govern the LTE case, although the setting of $H = 0$ is an extreme case of LTNE—this apparently contradictory state is brought about by having slightly different transformations in (8) and (9) from what is required for a single-temperature model. Nevertheless, this allows us to compare the two substantially different numerical methods with each other, with data from published papers, and with the analytical solution,

$$f(\eta) = f_w + \frac{1 - e^{-\tau\eta}}{\tau}, \quad \theta = e^{-\tau\eta}, \tag{20}$$

where

$$\tau = \frac{f_w + \sqrt{f_w^2 + 4}}{2}. \tag{21}$$

which was presented by Gupta and Gupta (1977). Thus, the reduced Nusselt number for this case is precisely τ. Comparisons are made in the following Table 1.

4 Results, Discussion and Analysis

In this section we present our numerical results and will try to be as comprehensive as possible, given that they are three parameters to vary, namely, f_w, H and γ.

4.1 Temperature Profiles

The effects of varying the suction/injection parameter on the dimensionless temperature profiles are presented in Fig. 2 for the case, $H = \gamma = 1$, which is a case for which LTNE effects are expected to be moderate. Four cases are shown, namely, $f_w = -5, 0, 5, 10$. Continuous lines depict the fluid temperature profile, θ, and the dashed curves that of the solid, ϕ.

It is quite clear to see that the profiles vary considerably in thickness as f_w varies. When f_w is large and negative, the boundary layer thicknesses are large, and the phases are almost in LTE. On the other hand, when f_w increases to large positive values, the thermal boundary layer of the fluid continues to get thinner, while that of the solid tends towards a constant thickness.

Table 1 Comparison of the present numerical values of $-\theta'(0)$ with those of other authors and the analytical solution when $H = 0$

f_w	Magyari & Keller	Cheng	Ali	Runge-Kutta	Keller box	Analytical
−1	0.6180	0.6180	0.61803	0.61803404	0.61803404	0.61803399
−0.8	0.6770	0.6770	0.67703	0.67703299	0.67703299	0.67703296
−0.4	0.8198	0.8198	0.81980	0.81980391	0.81980391	0.81980390
0	1.0000	1.0000	1.00000	0.99999985	1.00000000	1.00000000
1	1.6180	1.6180	1.61803	1.61803398	1.61803399	1.61803399

The Keller box computations used $\eta_{\max} = 20$ with 100 intervals and a grid expansion factor of 1.04, while the Runge-Kutta computations used a uniform grid of 400 intervals with the same value of $\eta_{\max}$

When f_w is large and negative there is a strong blowing from the surface, and this is clearly the physical reason why the boundary layer thickness also increases. The consequent reduction in the temperature gradient also means that it is easier for the phases to adopt the same local temperature. This situation may be analysed by replacing $f(\eta)$ by $f(\eta) + f_w$ in Eqs. (11)–(13). We obtain,

$$f'' = \theta', \tag{22}$$

$$\theta'' + f_w\theta' + f\theta' - f'\theta = H(\theta - \phi), \tag{23}$$

$$\phi'' = H\gamma(\phi - \theta). \tag{24}$$

In brief, if Eq. (23) is multiplied by γ and added to Eq. (24), and, guided by the numerical evidence, we set $\theta = \phi$. Then these two equations reduce to,

$$\frac{1+\gamma}{\gamma}\theta'' + f_w\theta + f\theta' - f'\theta = 0. \tag{25}$$

The system formed by this equation together with Eq. (22) has the solution,

$$f = \frac{1 - e^{-\delta\eta}}{\delta}, \quad \theta = e^{-\delta\eta}, \tag{26}$$

where δ is given by,

$$\delta = \frac{f_w + \sqrt{f_w^2 + 4(\gamma+1)/\gamma}}{2(\gamma+1)/\gamma}. \tag{27}$$

There is a strong resemblance between this solution and the one given in (20) and (21). Here $f_w \ll -1$, and therefore $\delta \sim -1/f_w$, which yields a very slow exponential decay, as may be seen in Fig. 2. The solution given by Eq. (26) for $f_w = -5$ and $H = \gamma = 1$ is indistinguishable graphically from the corresponding curve for θ in Fig. 2.

When the suction/injection parameter, f_w, is large and positive, the movement of the fluid towards the surface naturally causes the thermal boundary layer of the fluid phase to become thinner. However, Eq. (13) shows that the solid phase temperature field is not affected directly by the suction velocity but only indirectly via the source/sink term involving θ, and therefore heat may conduct freely away from the hot surface. Figure 2 suggests that the thickness of the thermal boundary layer for the solid is independent of f_w when $f_w \gg 1$. A summary of an asymptotic analysis of the $f_w \gg 1$ is given in Appendix A and this culminates in a

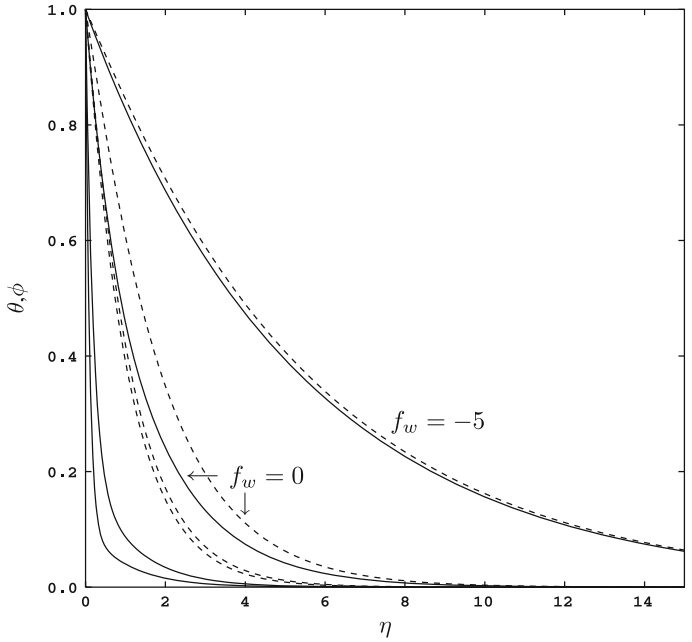

Fig. 2 Profiles of θ (*lines*) and ϕ (*dashes*) for the case, $H = \gamma = 1$, with $f_{\mathrm{w}} = -5, 0, 5, 10$

three-term solution for f, θ and ϕ, and the corresponding surface rates of heat transfer. This analysis also confirms the notion of a thinning boundary layer for the fluid phase and one of constant thickness for the solid phase as $f_{\mathrm{w}} \to \infty$.

Corresponding profiles of temperature for the cases, $H = 10$ and $H = 0.1$, with $\gamma = 1$, are shown in Figs. 3 and 4. The above observations also apply, although it is clear for the $H = 10$ case that the phases are effectively very close to LTE even when f_{w} is zero. When f_{w} increases from zero towards 10, it is only then that LTNE effects begin to be evident. On the other hand, when $H = 0.1$, even the $f_{\mathrm{w}} = -5$ solution is not yet in LTE, although the solutions will tend towards LTE as f_{w} becomes even more negative and blowing effects become stronger.

For the sake of brevity, we will omit the presentation of the effect of varying γ on the temperature profiles, but we note that large values of γ also cause the phases to act in LTE while LTNE dominates when γ takes small values. In this regard the qualitative behaviour is the same as when H varies for fixed values of γ.

4.2 Reduced Nusselt Numbers

Figures 5 and 6 depict how the reduced Nusselt numbers of the two phases vary with H when H lies in the range $10^{-2} \leq H \leq 10^{6}$, and these are compared with the large-H asymptotic results which are described briefly in Appendix B.

Figure 5 focusses on the case of mild suction, $f_{\mathrm{w}} = 1$, and curves of $\mathrm{Nu_f Ra}_x^{-1/2}$ and $\mathrm{Nu_s Ra}_x^{-1/2}$ are given for the three cases, $\gamma = 0.1,\ 1$ and 10. When H increases to large values we see that both $\mathrm{Nu_f Ra}_x^{-1/2}$ and $\mathrm{Nu_s Ra}_x^{-1/2}$ tend towards a common constant value which is given by the leading terms in Eqs. (53) and (54), and therefore the phases approach LTE. This approach is well-described by the asymptotic theory which is presented in Appendix B

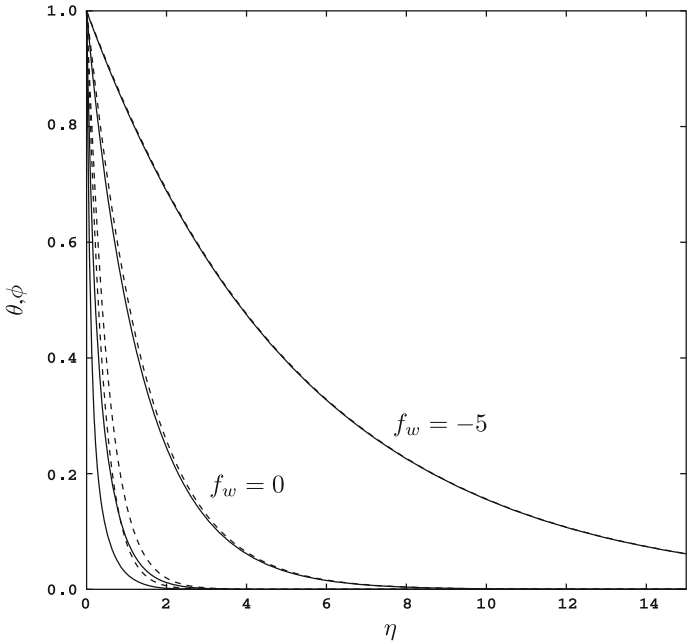

Fig. 3 Profiles of θ (*lines*) and ϕ (*dashes*) for the case, $H = 10,\ \gamma = 1$, with $f_{\mathrm{w}} = -5, 0, 5, 10$

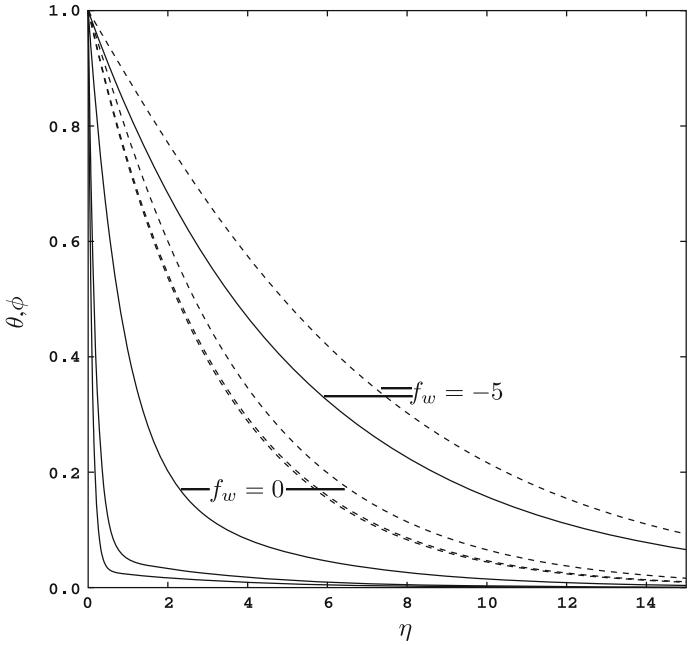

Fig. 4 Profiles of θ (*lines*) and ϕ (*dashes*) for the case, $H = 0.1,\ \gamma = 1$, with $f_{\mathrm{w}} = -5, 0, 5, 10$

and depicted as dotted curves in Fig. 5. On the other hand, when $H \to 0$, the source/sink terms in the governing equations become much less effective, and the respective reduced Nusselt numbers diverge. Figure 4, for which $H = 10$, shows that the thermal boundary layer

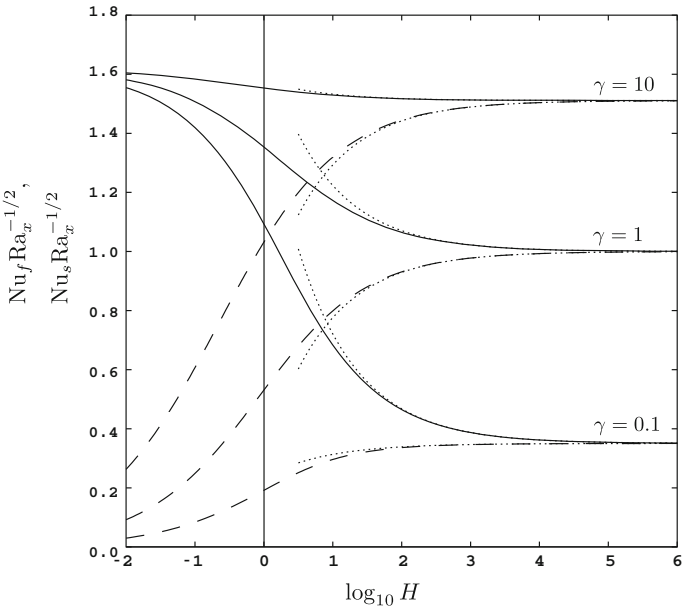

Fig. 5 Variation of $\mathrm{Nu_f Ra}_x^{-1/2}$ (*continuous lines*) and $\mathrm{Nu_s Ra}_x^{-1/2}$ (*dashed lines*) with $\log_{10} H$ for the case, $f_\mathrm{w} = 1$, with $\gamma = 0.1, 1, 10$. The *dotted lines* are the $H \gg 1$ asymptotic results

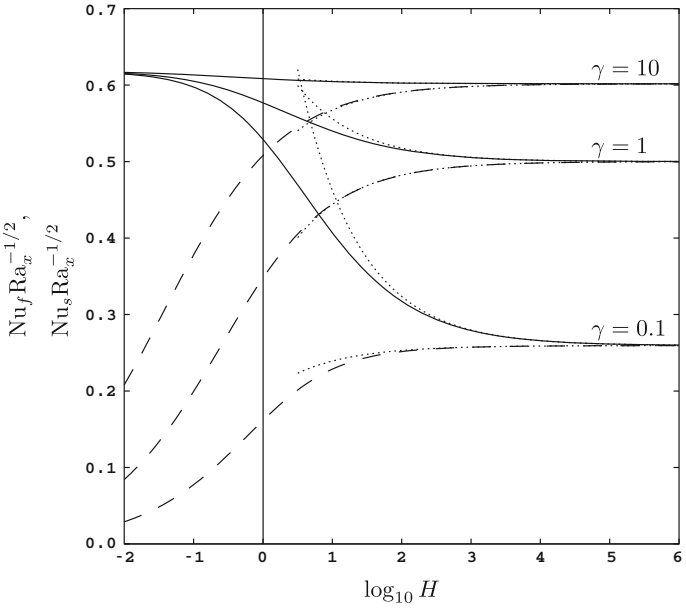

Fig. 6 Variation of $\mathrm{Nu_f Ra}_x^{-1/2}$ (*continuous lines*) and $\mathrm{Nu_s Ra}_x^{-1/2}$ (*dashed lines*) with $\log_{10} H$ for the case, $f_\mathrm{w} = -1$, with $\gamma = 0.1, 1, 10$. The *dotted lines* are the $H \gg 1$ asymptotic results

thickness for the solid phase is very thick when f_w is positive, which leads to a small value of $\mathrm{Nu_s}$, whereas most of the variation for the fluid phase temperature profile takes place close to $\eta = 0$, leading to a relatively large value of $\mathrm{Nu_f}$. This behaviour of the reduced Nusselt

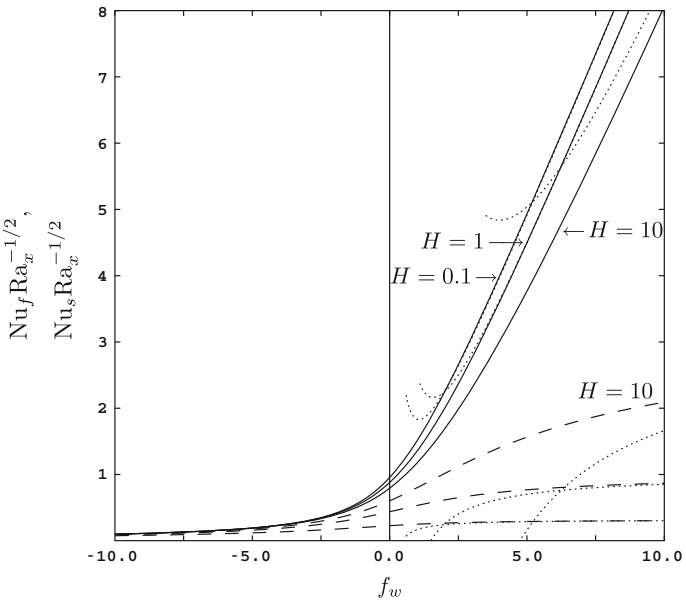

Fig. 7 Variation of $\mathrm{Nu_f Ra}_x^{-1/2}$ (*continuous lines*) and $\mathrm{Nu_s Ra}_x^{-1/2}$ (*dashed lines*) with f_w for the case, $\gamma = 1$, with $H = 0.1, 1, 10$. The *dotted lines* show the $f_\mathrm{w} \gg 1$ asymptotic results

number is seen clearly in Fig. 5 as $H \to 0$. Although we do not prove it here, it is not difficult to show that

$$\mathrm{Nu_f Ra}_x^{-1/2} \sim \tau \quad \text{and} \quad \mathrm{Nu_s Ra}_x^{-1/2} \sim \sqrt{H\gamma} \quad \text{when} \quad H \ll 1, \tag{28}$$

where τ is given in Eq. (21). The numerical values of $\mathrm{Nu_f Ra}_x^{-1/2}$ and $\mathrm{Nu_s Ra}_x^{-1/2}$ at $H = 10^{-2}$ in Fig. 2 are clearly in accord with these expressions.

Figure 6 shows the mild blowing counterpart to Fig. 5,s where we have taken $f_\mathrm{w} = -1$. Again, the same comments may be made about this case as for $f_\mathrm{w} = 1$. However, we have already seen that blowing causes the phases to approach LTE, and this means that $H = 10^{-2}$ is not yet small enough for $\mathrm{Nu}_s \mathrm{Ra}_x^{-1/2}$ to conform closely to the leading order value given in Eq. (28).

Figures 7 and 8 show the behaviour of $\mathrm{Nu_f Ra}_x^{-1/2}$ and $\mathrm{Nu_s Ra}_x^{-1/2}$ from the perspective of a varying f_w. Large negative values of f_w have been shown to lead to LTE (where $\mathrm{Nu_f} \simeq \mathrm{Nu_s}$) and the data used in drawing these figures confirm that fact, whereas large positive values lead to LTNE where $\mathrm{Nu_f} \gg \mathrm{Nu_s}$. It is also possible to see the presence of a two-layer structure in the fluid temperature profiles for the cases, $f_\mathrm{w} = 5$ and 10, in Fig. 4, where rapid exponential decay over a lengthscale which is of $O(f_\mathrm{w}^{-1})$ is followed by a slow decay over $O(1)$ lengthscales, as shown in Appendix A.

Figure 7 corresponds to $\gamma = 1$ with $H = 0.1$, 1 and 10, while Fig. 8 corresponds to $H = 1$ with $\gamma = 0.1$, 1 and 10. When $f_\mathrm{w} \gg 1$ we see the reduced Nusselt number for the fluid phase beginning to rise linearly, in line with Eq. (43). The analysis of Appendix A is based on the phases being under strong LTNE conditions, and therefore the comparison between the computed data and the asymptotic data is less good when $\gamma = 10$ in Fig. 7 and $H = 10$ in Fig. 8, because such large values of γ or H generally try to cause the phases to be in LTE. On the other hand, the $H = 0.1$ case in Fig. 7 and the $\gamma = 0.1$ case in Fig. 8

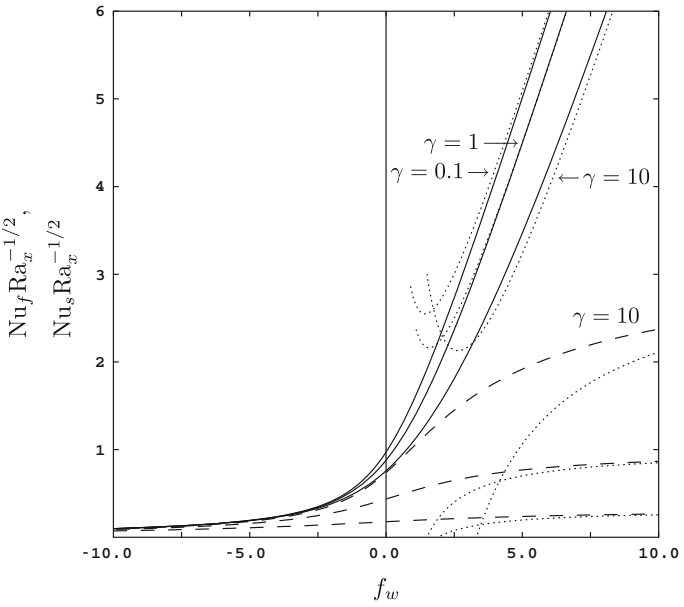

Fig. 8 Variation of $\mathrm{Nu_f Ra}_x^{-1/2}$ (*continuous lines*) and $\mathrm{Nu_s Ra}_x^{-1/2}$ (*dashed lines*) with f_w for the case, $H = 1$, with $\gamma = 0.1, 1, 10$. The *dotted lines* show the $f_\mathrm{w} \gg 1$ asymptotic results

match the asymptotic solutions very well, even when f_w is as low as five, which cannot be really regarded as being asymptotically large.

5 Conclusions

In the present paper we have considered the combined effects of LTNE, uniform surface suction/blowing and the presence of a linear variation of the surface temperature on buoyancy-induced flow from a vertical surface. The similarity solutions were solved numerically and have been supplemented by two detailed asymptotic analyses, one for $f_\mathrm{w} \to \infty$ and the other for $H \to \infty$. Brief mention has also been made in the paper of the cases, $f_\mathrm{w} \to -\infty$ and $H \to 0$. Other asymptotic limits are also possible such as, $H = O(1)$ and $\gamma \to \infty$, $H = O(1)$ and $\gamma \to 0$, $H\gamma = O(1)$ and $H \to \infty$, and $H\gamma = O(1)$ and $H \to 0$. Other less obvious possibilities also exist. Some of these require numerical solution, but all follow roughly the same type of methodology used in the two Appendices. Therefore we shall not consider them here, for reasons of space.

It has been found that LTE may be achieved in any of three possible separate limits, namely $H \to \infty$, $\gamma \to \infty$ and $f_\mathrm{w} \to -\infty$. The first two of these limits are well-known from other contexts, while the third, the strong blowing case, is not so obvious a priori. Strong LTNE effects are obtained in the opposite limits, namely when $H \to 0$, $\gamma \to 0$ or $f_\mathrm{w} \to \infty$. In these cases the thermal boundary layer splits into two, a relatively thin sublayer within which the fluid temperature drops from unity down to close to zero, and a relatively thick outer sublayer within which the temperature of the solid phase decreases to zero. Thus, the respective reduced Nusselt numbers of the phases are very different from one another in these limits.

Acknowledgements The authors would like to thank the anonymous reviewer for his/her very useful comments which have served to improve the paper.

Appendix A: Asymptotic Analysis for Large Values of f_w

We begin with Eqs. (22)–(24) where f has been replaced by $f + f_w$ in Eqs. (11)–(13). For the sake of completeness we quote these equations below,

$$f'' = \theta', \tag{29}$$

$$\theta'' + f_w\theta' + f\theta' - f'\theta = H(\theta - \phi), \tag{30}$$

$$\phi'' = H(\phi - \theta), \tag{31}$$

and note that the boundary conditions are the same as are given in (14) except that $f = 0$ at $\eta = 0$.

When f_w is large and positive, which corresponds to strong suction, then the two dominant terms in Eq. 30 must be the first two. A simple order-of-magnitude analysis shows that $f_w \gg 1$ corresponds to a lengthscale of $O(f_w^{-1})$, and this is the thickness of the thermal boundary layer of the fluid phase. On the other hand, Eq. (31) indicates that, apart from rapid variations when $\eta = O(f_w^{-1})$, the natural width of the thermal boundary layer of the solid phase is $O(1)$. Therefore, we need to adopt a matched asymptotic analysis where an inner region of width $O(f_w^{-1})$ is embedded within an outer region of with $O(1)$ width.

Let $\zeta = f_w\eta$ be the inner variable. In the inner region the three dependent variables are replaced by their uppercase counterparts. Therefore Eqs. (29)–(31) become,

$$f_w\ddot{F} = \dot{\Theta}, \tag{32}$$

$$f_w^2(\ddot{\Theta} + \dot{\Theta}) + f_w(F\dot{\Theta} - \dot{F}\Theta) = H(\Theta - \Phi), \tag{33}$$

$$f_w^2\ddot{\Phi} = H(\Phi - \Theta), \tag{34}$$

where the dots denote derivatives with respect to ζ. The two sixth order systems formed by Eqs. (29)–(31) and Eqs. (32)–(34) are to be solved subject to,

$$F = 0, \quad \Theta = \Phi = 1 \quad \text{at} \quad \zeta = 0, \tag{35}$$

$$f', \theta, \phi \to 0 \quad \text{as} \quad \eta \to \infty, \tag{36}$$

and asymptotic matching between the two regions.

All dependent variables are expanded as functions of either η or ζ as a power series in inverse integer powers of f_w. The analysis proceeds in a straightforward manner, with constants of integration and coefficients of complementary functions being found by asymptotic matching, and therefore we omit the details for the sake of brevity. We find that the solution in the inner region takes the form,

$$F(\zeta) \sim \left[1 - \mathrm{e}^{-\zeta}\right]f_w^{-1} + \left[\frac{H\gamma\zeta^2}{2} + \frac{H\zeta}{2} + H\gamma(1 - \mathrm{e}^{-\zeta})\right]f_w^{-2}, \tag{37}$$

$$\Theta(\zeta) \sim \mathrm{e}^{-\zeta} + \left(\frac{H}{\gamma}\right)^{1/2}\left[1-\mathrm{e}^{-\zeta}\right] f_{\mathrm{w}}^{-1} + \left[-H\zeta - (H+1)\zeta \mathrm{e}^{-\zeta} + H\left(\frac{2\gamma-1}{2\gamma}\right)\left(1-\mathrm{e}^{-\zeta}\right)\right] f_{\mathrm{w}}^{-2}, \tag{38}$$

$$\Phi(\zeta) \sim 1 - \left[\sqrt{H\gamma}\,\zeta\right] f_{\mathrm{w}}^{-1} + \left[H\gamma\left(\zeta^2/2 + 1 - \mathrm{e}^{-\zeta}\right) + H\zeta/2\right] f_{\mathrm{w}}^{-2}, \tag{39}$$

and the solution in the outer region takes the form,

$$f(\eta) \sim \left[1 + \frac{1}{\gamma}\left(1 - \mathrm{e}^{-\sqrt{H\gamma}\,\eta}\right)\right] f_{\mathrm{w}}^{-1}, \tag{40}$$

$$\theta(\eta) \sim \left[1 - \mathrm{e}^{-\sqrt{H\gamma}\,\eta}\right] f_{\mathrm{w}}^{-1} + \left[H\left(\frac{2\gamma-1}{2\gamma}\right)\mathrm{e}^{-\sqrt{H\gamma}\,\eta} + \frac{1}{2}\left(\frac{H^3}{\gamma}\right)^{1/2}\eta \mathrm{e}^{-\sqrt{H\gamma}\,\eta}\right] f_{\mathrm{w}}^{-2}, \tag{41}$$

$$\phi(\eta) \sim \mathrm{e}^{-\sqrt{H\gamma}\,\eta} + \left[\frac{H}{2}\eta \mathrm{e}^{-\sqrt{H\gamma}\,\eta}\right] f_{\mathrm{w}}^{-1}. \tag{42}$$

It is now possible to use Eqs. (38) and (39) to determine analytical expressions for the reduced Nusselt numbers for the large—f_{w} case:

$$\mathrm{Nu_f Ra}_x^{-1/2} \sim f_{\mathrm{w}} - \left(\frac{H}{\gamma}\right)^{1/2} + \left[1 + H + \frac{H}{2\gamma}\right] f_{\mathrm{w}}^{-1}, \tag{43}$$

$$\mathrm{Nu_s Ra}_x^{-1/2} \sim (H\gamma)^{1/2} - H(\gamma + {}^1\!/_2) f_{\mathrm{w}}^{-1}. \tag{44}$$

Appendix B: Asymptotic Analysis for Large Values of H

We begin with the modifed Eqs. (29) to (31) and we will consider the large-H behaviour of their solutions.

It is often true that, for convective flows in the presence of LTNE, the large-H analysis is composed of a straightforward series expansion in inverse integer powers of H; see Rees and Pop (1999) as an example of this. For the present flow the analysis is not so straightforward. We find that it is necessary to invoke a near-wall internal boundary layer of thickness of $O(H^{-1/2})$ to be able to satisfy the boundary conditions on the wall. We will refer to layer of $O(1)$ thickness as the outer layer, and the near-wall layer as the inner layer.

When $H \gg 1$ we expect the temperatures of the fluid and the solid to be equal at leading order. The form of Eqs. (29)–(31) suggests an outer layer solution in inverse powers of H:

$$\begin{pmatrix} f \\ \theta \\ \phi \end{pmatrix} = \sum_{n=0}^{\infty} \begin{pmatrix} f_n \\ \theta_n \\ \phi_n \end{pmatrix} H^{-n}. \tag{45}$$

On omitting the details of our calculations, we find that the solution correct to $O(H^{-1})$ is,

$$f \sim \frac{1-\mathrm{e}^{-\delta\eta}}{\delta} - \left[\frac{\delta^2}{\gamma(1+\gamma)}\eta \mathrm{e}^{-\delta\eta}\right] H^{-1}, \tag{46}$$

$$\theta \sim \mathrm{e}^{-\delta\eta} - \left[\frac{\delta^2}{\gamma(1+\gamma)}\left(1-\delta\eta\right)\mathrm{e}^{-\delta\eta}\right] H^{-1}, \tag{47}$$

$$\phi \sim \mathrm{e}^{-\delta\eta} - \Big[\frac{\delta^2}{\gamma(1+\gamma)}\Big(1-\delta\eta\Big)\mathrm{e}^{-\delta\eta} - \frac{\delta^2}{\gamma}\mathrm{e}^{-\delta\eta}\Big]H^{-1}. \tag{48}$$

In these solutions the value, δ, is given by,

$$\delta = \frac{f_\mathrm{w} + \sqrt{f_\mathrm{w}^2 + 4(\gamma+1)/\gamma}}{2(\gamma+1)/\gamma}, \tag{49}$$

which is the same as is given by Eq. (27). Under normal circumstances the $O(H^{-1})$ solution should satisfy the boundary conditions that both $\theta_{f,1}$ and $\theta_{s,1}$ are zero when $\eta = 0$, but it is not possible to do this simultaneously for the two dependent variables. It is for this reason that the inner layer has to be invoked.

An order of magnitude balance between the diffusion terms and the source/sink terms in (30) and (31) suggests that the inner variable,

$$\xi = H^{1/2}\eta, \tag{50}$$

should be used. Omitting details of the calculations, we find that the inner solutions mostly reflect the small-η Taylor series expansion of the outer solutions given above and are therefore passive. There is a deviation from this pattern at $O(H^{-1})$ which allows a large—ξ asymptotic match with the small—η expansion of the outer solutions. We find that the inner solutions for the temperatures are,

$$\theta \sim 1 - \delta\xi H^{-1/2} + \Big[-\frac{\delta^2}{\gamma(\gamma+1)}\Big(1-\mathrm{e}^{-\sqrt{\gamma+1}\,\xi}\Big) + \frac{\delta^2\xi^2}{2}\Big]H^{-1}, \tag{51}$$

$$\phi \sim 1 - \delta\xi H^{-1/2} + \Big[\frac{\delta^2}{\gamma} - \frac{\delta^2}{\gamma(\gamma+1)}\Big(1+\gamma\mathrm{e}^{-\sqrt{\gamma+1}\,\xi}\Big) + \frac{\delta^2\xi^2}{2}\Big]H^{-1}. \tag{52}$$

Therefore the reduced Nusselt numbers may now be computed from the inner layer solutions and are found to be,

$$\mathrm{Nu_f Ra}_x^{-1/2} = -\frac{\mathrm{d}\theta}{\mathrm{d}\eta}\Big|_{\eta=0} \sim \delta + \Big(\frac{\delta^2}{\gamma\sqrt{\gamma+1}}\Big)H^{-1/2}, \tag{53}$$

$$\mathrm{Nu_s Ra}_x^{-1/2} = -\frac{\mathrm{d}\phi}{\mathrm{d}\eta}\Big|_{\eta=0} \sim \delta - \Big(\frac{\delta^2}{\sqrt{\gamma+1}}\Big)H^{-1/2}. \tag{54}$$

Thus, the inner layer is manifested in the heat transfer results by having terms which are proportional to $H^{-1/2}$.

References

Ali, M.E.: The effect of lateral mass flux on the natural convection boundary layers induced by a heated vertical plate embedded in a saturated porous medium with internal heat generation. Int. J. Therm. Sci. **46**, 157–163 (2007)

Banu, N., Rees, D.A.S.: The onset of Darcy-Bénard convection using a thermal nonequilibrium model. Int. J. Heat Mass Transf. **45**, 2221–2228 (2002)

Baytaş, A.C., Pop, I.: Free convection in a square porous cavity using a thermal nonequilibrium model. Int. J. Therm. Sci. **41**, 861–870 (2002)

Cheng, P.: The influence of lateral mass flux on free convection boundary layers in a saturated porous medium. Int. J. Heat Mass Transf. **20**, 201–206 (1977)

Cheng, P., Chang, I.-D.: On buoyancy induced flows in a saturated porous medium adjacent to impermeable horizontal surfaces. Int. J. Heat Mass Transf. **19**, 1267–1272 (1976)

Cheng, P., Minkowycz, W.J.: Free convection about a vertical flat plate embedded in a porous medium with application to heat transfer from a dike. J. Geophys. Res. **82**, 2040–2044 (1977)
Combarnous, M., Bories, S.: Modelisation de la convection naturelle au sein d'une couche poreuse horizontal l'aide d'un coefficient de transfert solide–fluide. Int. J. Heat Mass Transf. **17**, 505–515 (1974)
Gupta, P.S., Gupta, A.S.: Heat and mass transfer on a stretching sheet with suction or blowing. Canad. J. Chem. Eng. **55**, 744–746 (1977)
Kuznetsov, A.V.: Thermal nonequilibrium forced convection in porous media. In: Ingham, D.B., Pop, I. (eds.) Transport Phenomena in Porous Media. Pergamon, Oxford (1998)
Magyari, E., Keller, B.: Exact analytical solutions for free convection boundary layers on a heated vertical plate with lateral mass flux embedded in a saturated porous medium. Heat Mass Transf. **36**, 109–116 (2000)
Mohamad, A.A.: Nonequilibrium natural convection in a differentially heated cavity filled with a porous matrix. Trans. ASME J. Heat Transf. **122**, 380–384 (2000)
Rees, D.A.S.: Vertical free convective boundary-layer flow in a porous medium using a thermal nonequilibrium model: elliptical effects. J. Appl. Math. Phys. (ZAMP) **54**, 437–448 (2003)
Rees, D.A.S.: Microscopic modelling of the two-temperature model for conduction in heterogeneous media: three-dimensional media. In: Proceedings of the 4th International Conference on Applications of Porous Media, Paper 15, Istanbul (2009)
Rees, D.A.S.: Microscopic modeling of the two-temperature model for conduction in heterogeneous media. J. Porous Media **13**, 125–143 (2010)
Rees, D.A.S., Bassom, A.P.: The radial injection of a hot fluid into a cold porous medium: the effects of local thermal non-equilibrium. Comput. Therm. Sci. **2**(3), 221–230 (2010)
Rees, D.A.S., Bassom, A.P., Siddheshwar, P.G.: Local thermal non-equilibrium effects arising from the injection of a hot fluid into a porous medium. J. Fluid Mech. **594**, 379–398 (2008)
Rees, D.A.S., Pop, I.: Free convective stagnation point flow in a porous medium using a thermal nonequilibrium model. Int. Commun. Heat Mass Transf. **26**, 945–954 (1999)
Rees, D.A.S., Pop, I.: Vertical free convective boundary-layer flow in a porous medium using a thermal nonequilibrium model. J. Porous Media **3**, 31–44 (2000)
Rees, D.A.S., Pop, I.: Local thermal nonequilibrium in porous medium convection. In: Ingham, D.B., Pop, I. (eds.) Transport Phenomena in Porous Media III, pp.147–173. Pergamon, Oxford (2005)